J Appl Electrochem (2016) 46:975–985
DOI 10.1007/s10800-016-0972-y

RESEARCH ARTICLE

Photovoltaic study of quantum dot-sensitized TiO_2/CdS/ZnS solar cell with P3HT or P3OT added

Andrea Cerdán-Pasarán[1,2] · Diego Esparza[1] · Isaac Zarazúa[1,3] · Manuel Reséndiz[1,4] · Tzarara López-Luke[1] · Elder De la Rosa[1] · Rosalba Fuentes-Ramírez[2] · Alejandro Alatorre-Ordaz[2] · Alejandro Martínez-Benítez[1]

Received: 8 January 2016 / Accepted: 5 May 2016 / Published online: 14 May 2016

Abstract Within the body of research aimed at improving the photovoltaic performance of quantum dot-sensitized solar cells (QDSSC), poly-3-alkyl thiophenes have been commonly used in hybrid photovoltaic devices. The roles of poly(3-hexylthiophene) (P3HT) and of poly(3-octylthiophene) (P3OT) on hybrid QDSSC were investigated in the present work. To this end, CdS and ZnS QDs were deposited by successive ionic layer adsorption and reaction method on TiO_2 mesoporous film. The polymers were added by drop-casting method giving the configurations TiO_2/CdS/ZnS/P3HT and TiO_2/CdS/ZnS/P3OT. Results showed that the polymer covers the TiO_2/CdS/ZnS surface enough to protect it from contact with the polysulfide electrolyte, while electrochemical impedance spectroscopy measurements indicated that when P3HT and P3OT were employed, the recombination resistance increased and the transport resistance decreased, causing the improvement of the open circuit voltage and fill factor, respectively.

Graphical Abstract

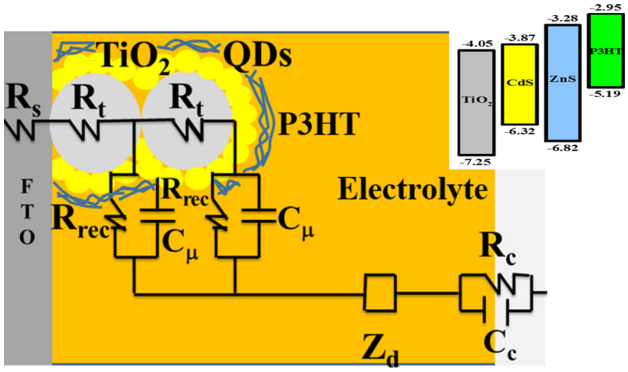

Keywords P3HT · P3OT · Hybrid quantum dot-sensitized solar cells · CdS · TiO_2

1 Introduction

Global environmental concerns and the increased consumption of fossil fuels to meet the world growing energy demand are opening up new opportunities for research on alternative energy sources. The sun represents the cleanest, the most abundant, and inexhaustible source of renewable energies, and solar cells are the promising means for tapping into this kind of limitless energy source [1, 2]. Among the different types of solar cells currently developed, those based on nanostructured materials are classified in three categories: organic cells based on molecules or semiconducting polymers sensitized with carbon nanomaterials [3–6]; inorganic cells based on inorganic semiconductor nanomaterials sensitized with another semiconductor [7–10]; and hybrid solar

✉ Tzarara López-Luke
tzarara@cio.mx

1 Centro de Investigaciones en Óptica, A.P 1-948, 37150 León, Gto, Mexico

2 División de Ciencias Naturales y Exactas, Universidad de Guanajuato, Noria Alta s/n, 36050 Guanajuato, Gto, Mexico

3 Institute of Advanced Materials, Universitat Jaume I, 12071 Castelló, Spain

4 Universidad Tecnológica del Estado de Querétaro (UTEQ), 76148 Santiago De Querétaro, Qro, Mexico

cells based on organic–inorganic nanostructures that combine the best properties of individual component in each system and thus achieve improved efficiency as the result of synergetic effects [11–17].

Inorganic quantum dot-sensitized solar cells (QDSSC) present advantages such as tunable band gaps to collect light from the visible to infrared spectrum [10, 18–21], high molar extinction coefficients [22], and multiple exciton generation [23–25]; all of which allow these cells to reach theoretical efficiencies as high as 44 % [26, 27]. So far, the power conversion efficiency achieved by these cells is 8 % [28]. Moreover, one of the most promising advantages of the nanostructured solar cells is the manipulability of factors, such as particles' shape and size, which improves the conversion efficiency as a result of quantum confinement [29–31]. Another key factor in conversion efficiency enhancement is improved electron and hole mobility to avoid recombination processes and increase the charge transport in the solar cell [32]. QDSSCs based on cadmium chalcogenide (CdS, CdSe, or CdTe) exhibit high capacity for efficiently absorbing photons in the visible region, as well as a band gap above 1.4 eV, and hence their significant advances in research. CdS quantum dots (QDs) are reported to be relatively stable, and have shown a modest 2 % efficiency in QDSSCs [33–35].

Likewise, photovoltaic devices made from conductive polymers have the advantage of tunable energy levels by modification of their chemical structure [36]. Also, they offer flexibility with the possibility for integration into building materials and solar devices [37]. However, their performance is limited by low mobility of charge carriers. It has been pointed out that the combination of semiconductor nanoparticles such as CdSe, CdS, PbS, and SiO_2 and polymers can improve the quantum efficiency of the solar cells [36, 38–40]. In trying to incorporate the inorganic nanomaterials into the polymers, several strategies have been followed, for example, ligand exchange, in situ synthesis of the QDs, and interconnected networks; still, these hybrid devices have low power conversion efficiencies [41]. An efficiency of 4.1 % was recently reported to have been obtained with a hybrid bulk heterojunction (BHJ) solar cell using CdS QDs capped with n-butylamine and blended with poly(3-hexylthiophene) (P3HT) nanowires [42]. Concerning the role of each material, discrepant results have been published by different research groups, but this is understandable given the complexity of a system that incorporates several polymers in a hybrid cell. P3HT, among the different varieties of poly-3-alkyl thiophenes, is the most widely used π-conjugated polymer for photovoltaic applications, followed by poly(3-octylthiophene) (P3OT) [43, 44].

In this work, the photoelectrochemical characteristics of hybrid QDSSC were studied using P3HT or P3OT organic polymer on a well-known TiO_2/CdS/ZnS arrangement in order to recognize the role of these polymers in the performance of this kind of solar cells. Indeed, photoconversion efficiency improved substantially, to around 33 %, with the addition of the conductor polymers varying from 2.2 % in the reference cell (TiO_2/CdS/ZnS) to 3 % in the configurations: TiO_2/CdS/ZnS/P3HT and TiO_2/CdS/ZnS/P3OT. This enhanced efficiency is a result of the increase of fill factor (FF) and open circuit voltage (V_{oc}) associated with the reduction of transport resistance and recombination, as demonstrated by impedance measurements. The differences between the cells with P3HT and those with P3OT were a better coating of the TiO_2/CdS/ZnS with P3HT, resulting in higher short circuit current (J_{sc}), and obtaining higher V_{oc} and FF with P3OT.

2 Experimental

In order to study the effects of the two polymers on the QD-sensitized TiO_2, three samples were fabricated: (1) TiO_2/CdS/ZnS, (2) TiO_2/CdS/ZnS/P3HT, and (3) TiO_2/CdS/ZnS/P3OT as follows.

2.1 Quantum dot-sensitized solar cells preparation

2.1.1 Materials

TiO_2 paste WER2-O Reflector and DSL 18NR-T were obtained from DYESOL, titanium(IV) isopropoxide (97 %), acetylacetone (>99 %), cadmium acetate dihydrate ($Cd(CH_3COO)_2 \bullet 2H_2O$), zinc acetate dihydrate ($Zn(CH_3COO)_2 \bullet 2H_2O$), sodium hydroxide (NaOH), tetra-*n*-butylammonium hexafluorophosphate ($TBAPF_6$), P3HT, and P3OT were obtained from Sigma-Aldrich. Sulfur (S) and sodium sulfide ($Na_2S \bullet 9H_2O$) were obtained from KARAL. Fluorine-doped tin oxide glasses (FTO, TEC-15) were purchased from MTI.

2.1.2 TiO_2 film Preparation

Fluorine-doped tin oxide glasses were cleaned with water, acetone, and ethanol in an ultrasonic bath for 15 min each before use. The photoelectrodes consist of three different TiO_2 layers, stacked one on the top of the other. The first TiO_2 film deposited was the compact layer. A solution of titanium(IV) isopropoxide (0.2 M) using acetylacetone/ethanol (V:V = 1:1) was deposited by spray pyrolysis over FTO and sintered at 450 °C for 30 min obtaining a 150-nm layer. The second layer was the transparent layer, prepared with TiO_2 paste (DSL 18-NRT) deposited by Doctor Blade method obtaining an 8-μm-thick layer. The third TiO_2 film (Wer2-O Reflector paste) was the scattering layer (opaque),

consisting in a 9.5-μm layer obtained by Doctor Blade deposition method. These films were sintered for 30 min at 450 °C to obtain good electrical contact between nanoparticles.

2.1.3 Films' sensitization

The TiO_2 electrode films were sensitized by successive ionic layer adsorption and reaction (SILAR) method using 0.05 M $Cd(CH_3COO)_2 \bullet 2H_2O$ dissolved in ethanol and 0.05 M Na_2S in methanol:water (V:V = 1:1) as Cd^{2+} and S^{2-} sources, respectively. A single SILAR cycle consisted of 1-min dip-coating the TiO_2 electrode into the cadmium acetate and subsequently into the sodium sulfide solutions, also for 1 min. Between successive dipping steps in precursor solutions, the electrodes were thoroughly rinsed by immersion in the corresponding solvent (ethanol and methanol/H_2O, respectively) in order to remove the excess content of precursor. Seven SILAR cycles were performed to obtain a uniform coverage of the TiO_2 NPs with CdS QDs. To enhance the photovoltaic performance, ZnS was deposited by SILAR to passivate CdS surface and to reduce the recombination of electrons from the TiO_2 to the polysulfide electrolyte [45–47]. ZnS was obtained from 0.1 M $Zn(CH_3COO)_2 \bullet 2H_2O$ and 0.1 M Na_2S both dissolved in water, using them as Zn^{2+} and S^{2-} sources, respectively. The films were dipped for 1 min/dip in the solutions during two SILAR cycles. Finally, the P3HT and P3OT were deposited by the drop-casting method: this technique consists in spreading evenly a drop (10 μl) of P3HT 10^{-7} M (or P3OT) in toluene onto TiO_2/CdS/ZnS films and drying for 10 min at room temperature.

2.1.4 Counter electrode fabrication and cell assembling

Cu_2S counter electrodes were obtained by immersing a brass foil in HCl solution (38 vol%) at 90 °C for 1 h, and then they were sulfated by adding a drop (20 μl) of polysulfide electrolyte. The composition of the polysulfide electrolyte was 1.0 M Na_2S, 1.0 M S, and 0.1 M NaOH, using deionized water. The solar cells were constructed by assembling the Cu_2S counter electrode and sensitized TiO_2 film electrode with a binder clip separated by a Scotch spacer. The polysulfide electrolyte was filled inside the cell.

2.2 Characterization

Field emission scanning electron microscopy (FE-SEM) images were obtained on a JEOL JSM-7800F microscope. The UV–Vis absorption spectra of P3HT and P3OT were measured by transmittance, and substrates were measured by diffuse reflectance in the range from 360 to 800 nm using an Agilent Technologies Cary Series UV–Vis–NIR spectrophotometer (Cary 5000) with an integrating sphere of 60 mm. The current density curves were measured using a Gamry reference 600 potentiostat/galvanostat. The samples were illuminated using an Oriel Sol 3A solar simulator while measuring current. The light intensity was adjusted employing a NREL-calibrated Si solar cell having KG-2 filter for one sun light intensity (100 mW cm^{-2}). Incident photon-to-current conversion efficiency (IPCE) spectra were measured using a monochromator Newport model 74125. Electrochemical impedance spectroscopy (EIS) measurements were carried out by applying a small voltage perturbation (10 mV) at frequencies ranging from 100 kHz to 0.1 Hz for different forward bias voltages under dark conditions. The energy levels of the semiconductors were calculated also by EIS, with a three-electrode cell, using each material present in the photoanode as working electrode. Ag/AgCl and Pt wires were the reference and counter electrode, respectively, and a solution of 1 M Na_2S was used as electrolyte. The fittings of the results were carried out using the ZView software. HOMO and LUMO levels of the polymers were calculated by cyclic voltammetry. The polymer films were deposited by the drop-casting method described above on FTO and were used as working electrode in 0.1 M $TBAPF_6$ in acetonitrile electrolyte. The reference and counter electrode were the same.

3 Results

3.1 Morphological characterization

The morphology of the photoanode is shown in SEM images, (see Fig. 1). The TiO_2 compact layer presented in Fig. 1a is formed of clusters around 150-nm size. Also, a homogeneous, highly porous TiO_2 transparent layer composed of particles with an average size of 20 nm is shown in Fig. 1b. Figure 1c shows the TiO_2 scattering layer. This film has a larger particle size (400 nm). Figure 1d demonstrates a good coverage of the CdS QDs over the TiO_2 surface. The TiO_2 film with CdS/ZnS QDs and P3HT is presented in Fig. 1e. Herein is observed that the particles agglomerate on the surface to form rods probably due to the P3HT deposited. In Fig. 1f, the P3OT deposited is observed as big clusters (of size 100 nm) wrapping the TiO_2/CdS/ZnS particles.

SEM image and EDS map of the cross-sectional photoanode TiO_2/CdS/ZnS/P3HT are shown in Fig. 2. The FTO/glass substrate has a thickness of 150 nm as observed on the left side of the SEM image. Adjacent to the TiO_2 compact layer is the FTO. Next are located the TiO_2 active layer which has 8-μm thickness and the TiO_2 scattering layer with 9.5-μm thickness. A homogeneous distribution

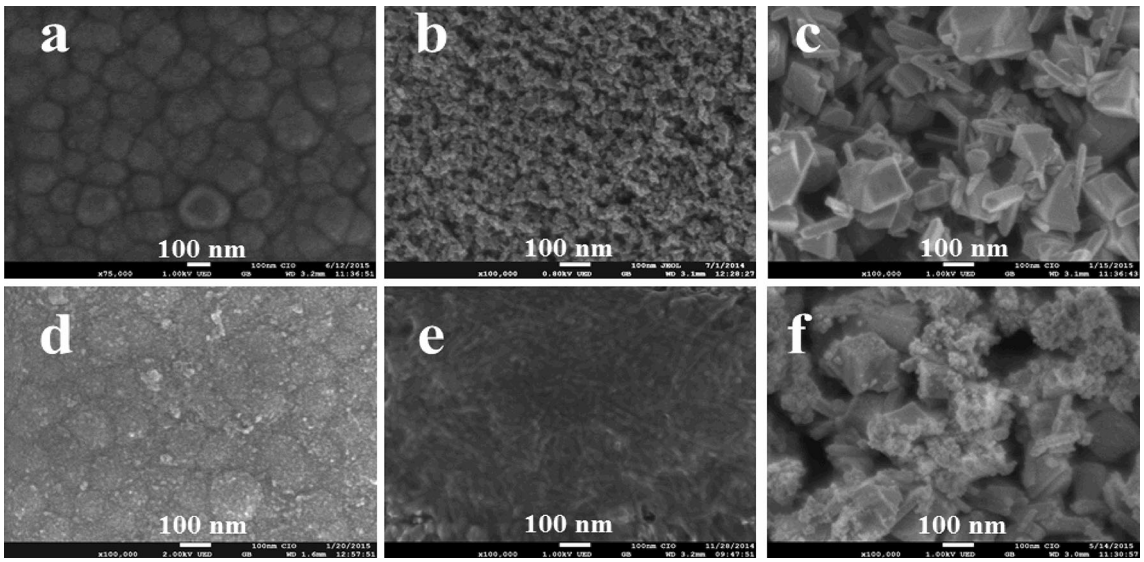

Fig. 1 SEM images of the morphology of each TiO_2 films **a** TiO_2 (compact layer), **b** TiO_2 (transparent layer), **c** TiO_2 (scattering layer); and the films **d** TiO_2/CdS/ZnS, **e** TiO_2/CdS/ZnS/P3HT, and **f** TiO_2/CdS/ZnS/P3OT

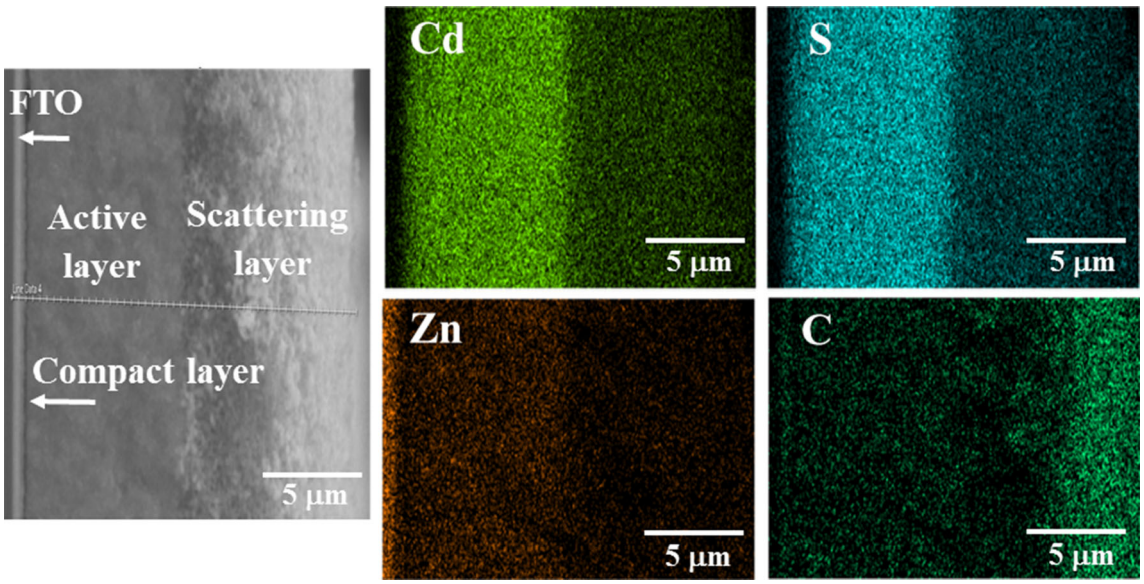

Fig. 2 SEM image and EDS distribution of the cross sectional photoanode with the TiO_2/CdS/ZnS/P3HT array

of Cd, S and Zn on the TiO_2 active layer is observed. Considering that the TiO_2 active layer has smaller-sized nanoparticle than the TiO_2 scattering layer, and that the CdS and ZnS QDs were added before the polymers, there is a bigger distribution of these QDs on the active layer. The largest distribution of the polymer was observed over the TiO_2 scattering layer; this is related to the polymer not being able to penetrate the surface formed between the QDs and the TiO_2 active layer, therefore it stays on the TiO_2 scattering layer. The behavior of TiO_2/CdS/ZnS/P3OT is very similar.

3.2 Optical absorption

The absorption spectra of the cells and the polymers are shown in Fig. 3. The TiO_2 film absorbs light on the short wavelength region centered at 350 nm, (Fig. 3a). The P3HT and the P3OT dispersed in toluene present a peak at 450 nm, however, P3HT has an absorption light up to 620 nm, while P3OT to 560 nm, see the inset figure. The TiO_2/CdS/ZnS cell shows in Fig. 3b an absorption band centered at 430 nm. This light absorption corresponds to the CdS QDs [48, 49], while the absorption peak at 375 nm

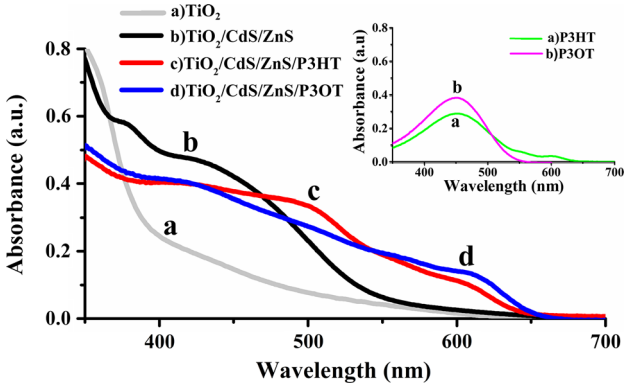

Fig. 3 Absorption spectra of **a** TiO_2, **b** TiO_2/CdS/ZnS, **c** TiO_2/CdS/ZnS/P3HT, and **d** TiO_2/CdS/ZnS/P3OT arrays. The *inset* shows absorption spectra of (*a*) P3HT and (*b*) P3OT in toluene

is related to the ZnS QDs [50, 51]. Moreover, by introducing the polymers to the cell the light absorption increases, for example the UV–Vis spectrum for the TiO_2/CdS/ZnS/P3HT film shows two absorption peaks (Fig. 3c), one at 500 nm and another at 605 nm. Likewise, the TiO_2/CdS/ZnS/P3OT film shows one absorption peak at 415 nm and a second peak at 605 nm, see Fig. 3d.

3.3 Photovoltaic characterization

The current density-voltage (*J–V* curves) are analyzed for the three configurations; TiO_2/CdS/ZnS, TiO_2/CdS/ZnS/P3HT and TiO_2/CdS/ZnS/P3OT, (see Fig. 4). The photovoltaic parameters as J_{sc}, V_{oc}, FF, and efficiency (η) are summarized in Table 1. The FF and η were calculated using Eqs. 1 and 2.

$$\mathrm{FF} = \frac{P_{\max}}{J_{sc} V_{oc}} \times 100, \tag{1}$$

$$\eta = \frac{P_{\max}}{P_i} \times 100 = \mathrm{FF}\frac{J_{sc} V_{oc}}{P_i}, \tag{2}$$

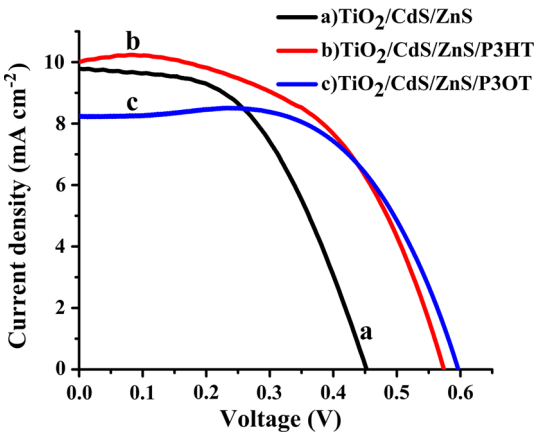

Fig. 4 *J–V* characteristic curves of the configurations **a** TiO_2/CdS/ZnS, **b** TiO_2/CdS/ZnS/P3HT, and **c** TiO_2/CdS/ZnS/P3OT

Table 1 Photocurrent, voltage, fill factor, and photoconversion efficiency values of the hybrid QDSSCs

Sample	J_{sc} (mA cm^{-2})	V_{oc} (V)	FF (%)	η (%)
TiO_2/CdS/ZnS	9.8	0.453	50.5	2.24
TiO_2/CdS/ZnS/P3HT	10.0	0.573	53.6	3.07
TiO_2/CdS/ZnS/P3OT	8.3	0.597	60.7	3.0

where $P_{\max}$ is the maximum obtainable power and P_i is the incident solar power. The *J–V* curves show the effect of P3HT or P3OT over CdS/ZnS QD-sensitized TiO_2. The V_{oc} increase from 0.453 V (TiO_2/CdS/ZnS) to 0.573 V and 0.597 V adding P3HT and P3OT, respectively. However, the J_{sc} of the TiO_2/CdS/ZnS cell (9.8 mA cm^{-2}) decreased to 8.3 mA cm^{-2} with the polymer P3OT addition. Another effect observed with the addition of P3HT and P3OT to the configuration TiO_2/CdS/ZnS was the improvement of the FF. The configuration TiO_2/CdS/ZnS has a FF of 50.5 % and an efficiency of 2.24 %. With the addition of the polymer P3HT to the cell, the FF increased to 53.6 %, and consequently, the η increased to 3.07 %. When P3OT was added, the FF increased even more than with the P3HT to 60.7 %, with no increase in efficiency (3 %). In spite of the variations in the V_{oc} and J_{sc}, the efficiencies for the TiO_2/CdS/ZnS/P3OT and TiO_2/CdS/ZnS/P3HT cells are the same due to the high FF of the TiO_2/CdS/ZnS/P3OT array.

The IPCE characterization provides a measurement of the number of electrons that are photogenerated for each incident photon at a given wavelength (λ) and can be determined from the J_{sc}, using the expression 3 [52].

$$\mathrm{IPCE} = \frac{1240 \times J_{sc}}{\lambda \times I} \times 100. \tag{3}$$

The IPCE curves of the TiO_2/CdS/ZnS, TiO_2/CdS/ZnS/P3HT and TiO_2/CdS/ZnS/P3OT cells are shown in Fig. 5. The sample TiO_2/CdS/ZnS has an external quantum efficiency (or IPCE) of 90 % at 480 nm. Adding the polymers decreases the IPCE at this wavelength. For TiO_2/CdS/ZnS/P3HT, a decrease of the IPCE to 83 % is observed, and with the configuration TiO_2/CdS/ZnS/P3OT the IPCE is 78 %, this reduction is evidenced by the decreased J_{sc}. However, with the introduction of the polymers at longer wavelengths (up to 575 nm), the IPCE is higher.

Figure 6 shows a schematic band energy diagram for the configurations TiO_2/CdS/ZnS/P3HT and TiO_2/CdS/ZnS/P3OT cells. The conduction bands (CB) of TiO_2, CdS, and ZnS QDs are −4.05, −3.87, and −3.28 eV, respectively, and they were calculated from the analysis of the Mott-Schottky curves as was pointed previously [51]. From EIS measurements of a three-electrode cell configuration, the capacitance was estimated, and with the intercept in the *x*-axis of the Mott-Schottky plot, the flatband potential was obtained [53, 54]. The highest occupied molecular orbital

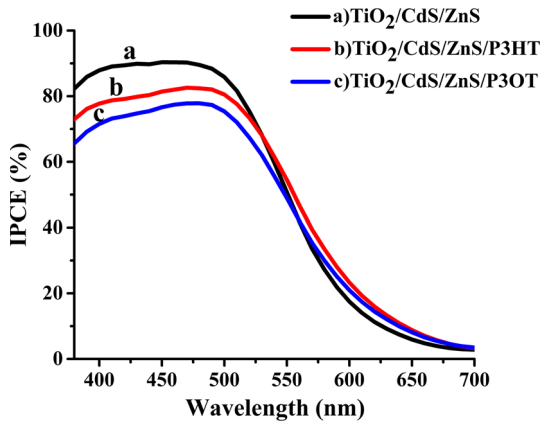

Fig. 5 IPCE spectra of the solar cells with the configuration: TiO_2/CdS/ZnS, TiO_2/CdS/ZnS/P3HT and TiO_2/CdS/ZnS/P3OT

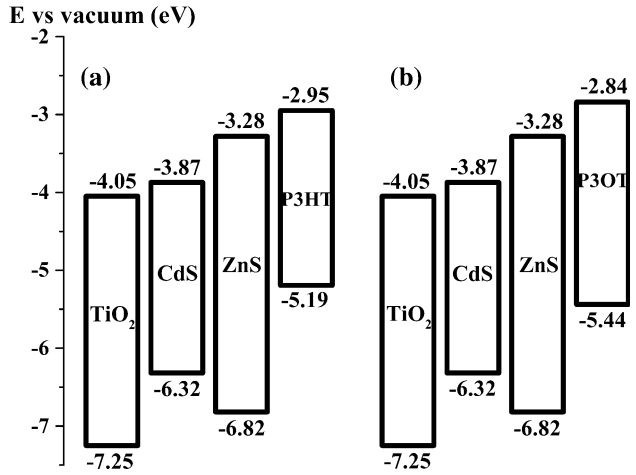

Fig. 6 Scheme illustrating energy levels of **a** TiO_2/CdS/ZnS/P3HT and **b** TiO_2/CdS/ZnS/P3OT arrays

(HOMO) for P3HT is −5.19 eV, and the lowest unoccupied molecular orbital (LUMO) is −2.95 eV, and for P3OT, the corresponding values are −5.44 and −2.84 eV, respectively. The HOMO and LUMO were estimated from Eqs. 4 and 5 [55–57]. The onset of oxidation (E_{ox}) were calculated from cyclic voltammetry curves, and E_g is the optical band gap obtained from the derivatives of the absorption spectra. The band gaps were 3.2 eV for TiO_2, 2.45 eV for CdS, 3.54 eV for ZnS QDs, 1.94 eV for P3HT and 2.3 eV for P3OT.

$$\text{HOMO} = -e(E_{ox} + 4.71)\text{eV}, \quad (4)$$

$$\text{LUMO} = E_g + 0.3 + \text{HOMOeV} \ . \quad (5)$$

3.4 Electrochemical impedances

EIS measurements were carried out to explain the variation of the electrochemical parameters in terms of the internal physical mechanism when CdS QDs and P3HT or P3OT are combined. The transmission line model indicated in Fig. 7 was used to fit the impedance measurements [58, 59]. There, R_s stand for the series resistance and is related to the FTO and the wires resistance, R_t is the transport resistance, and is related to the resistance of TiO_2 to the electron flux, R_{rec} and C_μ are the recombination resistance and the chemical capacitance, respectively. Z_d is the Warburg element showing the Nernst diffusion of the electrolyte; R_c and C_c are the charge-transfer resistance and double-layer capacitance at the counter electrode.

The impedance spectra of the sample TiO_2/CdS/ZnS measured at different potentials under dark conditions are presented in Fig. 8a, while the impedance spectra for TiO_2/CdS/ZnS, TiO_2/CdS/ZnS/P3HT, and TiO_2/CdS/ZnS/P3OT at 350 mV bias are shown in Fig. 8b. These spectra show the typical behavior of a large semicircle in the low-frequency region and a straight line in the high-frequency region [59, 60].

Figure 9 shows C_μ, R_{rec}, and R_t of the TiO_2/CdS/ZnS, TiO_2/CdS/ZnS/P3HT, and TiO_2/CdS/ZnS/P3OT solar cells extracted from the fitted EIS measurements. $C\mu$ is plotted as a function of $V_F = V_{app} - V_{series}$ which is the voltage drop at the active electrode obtained as the applied voltage, V_{app}, corrected by the voltage drop due to series resistance (V_{series}) [58, 59]. The chemical capacitance does not change as shown in Fig. 9a. An increase in the recombination resistance was observed when P3HT or P3OT was used (Fig. 9b), while the transport resistance decreased, Fig. 9c.

4 Discussion

4.1 Photoanode morphology

The TiO_2 compact layer was deposited on the FTO surface before the TiO_2 mesoporous layer to achieve higher

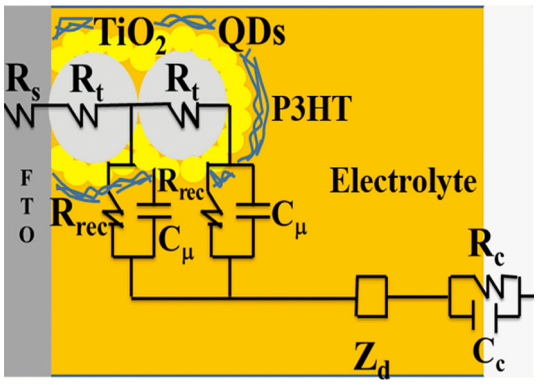

Fig. 7 Equivalent circuit employed in the QDSSC. R_s and R_t are the series resistance and transport resistance, respectively; Z_d is the Warburg element; R_c is the charge-transfer resistance; C_c is the double-layer capacitance; R_{rec} is the recombination resistance; and C_μ is the chemical capacitance

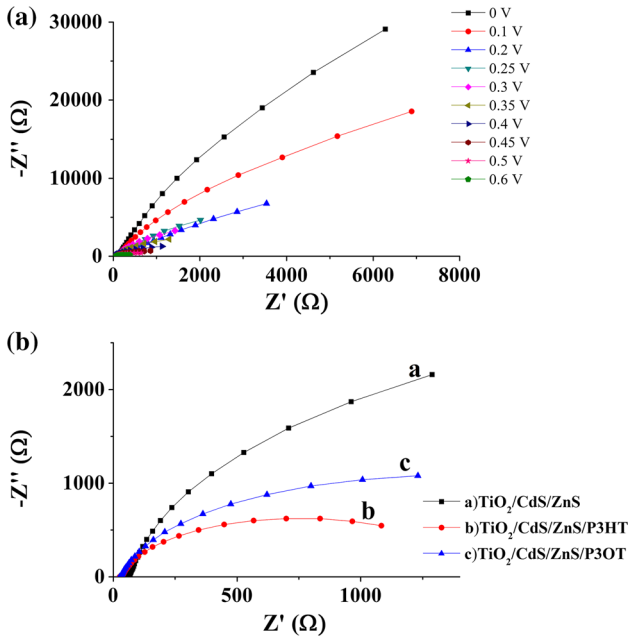

Fig. 8 Impedance spectra of **a** the TiO_2/CdS/ZnS cell at different potentials; and **b** the TiO_2/CdS/ZnS, TiO_2/CdS/ZnS/P3HT, and TiO_2/CdS/ZnS/P3OT at 350 mV

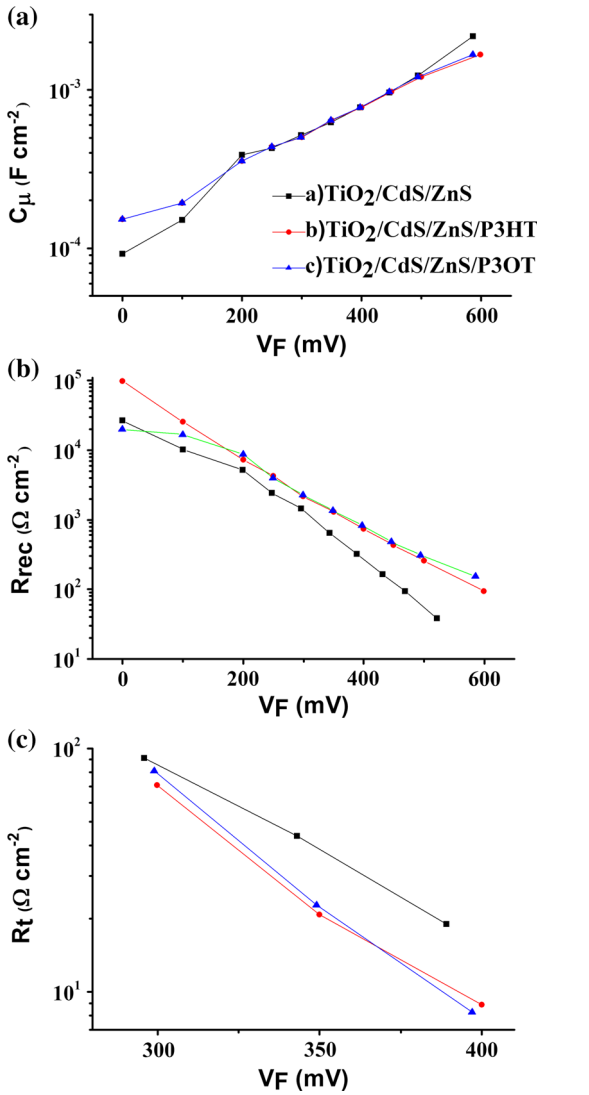

Fig. 9 Behaviors of the different parameters of the QDSSC obtained by EIS: **a** chemical capacitance, C_μ; **b** recombination resistance, R_{rec}; and **c** transport resistance, R_t

photovoltage as it blocks the contact of the FTO surface and the electrolyte [27]. The TiO_2 active layer, due to the small nanoparticles, has a large active area which helps to obtain high quantity of QDs deposited. The TiO_2 scattering layer increases light scattering, and thus, light harvesting due to the large particles ensures adequate light trapping in the device, increasing the absorption path length of photons and optical confinement [58, 61]. As the QDSSCs' performance depends on the film thickness, a balance among light scattering, QD loading, and recombination is necessary to optimize the performance. It has been reported that TiO_2 scattering layers as thick as 11 μm still can scatter incident light within the film and return it to the surface, contributing to the improvement of the solar cells' performance [62, 63].

SEM images confirm good coverage of CdS QDs deposited over TiO_2 porous film using SILAR method. The morphology of the photoanode when polymers were deposited changed from nanorods with P3HT to disordered agglomerated spheres with P3OT. A similar effect was noted elsewhere [3]. The photoanode covered with P3HT was more uniform. The distribution of the polymer in the TiO_2 layers indicates its good penetration, and as good interfacial contact is essential to maximize the interfacial areas and minimize the recombination of the charge carrier, it contributes to the enhancement of the fill factor [17].

The CdS QDs have light absorption in the visible region [35]. The ZnS QDs act as a barrier at the interface between the CdS QDs and the electrolyte, leading to the hindered recombination rate, but it does not contribute to light absorption [47, 50]. From the IPCE measurements, it can be observed that these polymers do not contribute to the light absorption considerably, as demonstrated by the decreased J_{sc}. Nevertheless, it has been established that the increment of absorption in hybrid QDSSCs is associated to the light-trapping effect produced by increased incident photon scattering within the polymeric network [36], which could be related to the enhanced absorption observed in TiO_2/CdS/ZnS when the polymers were incorporated (Fig. 3). Moreover, the polymers facilitate the hole transport and act as a potential barrier, as shown in the energy scheme, leading to a better electron–hole transport balance [32, 64].

4.2 Electrochemical performance

The unusual shape of the *J–V* curve (Fig. 4) for the TiO_2/CdS/ZnS/P3HT and TiO_2/CdS/ZnS/P3OT could be related with the hysteresis phenomenon. This behavior, observed in different kinds of solar cells, has been associated with trapping of charge carriers, ferroelectricity, ion migration, or ionic polarization [65–67]. According to the hybrid-QDSSC studied in this work, it is probable that the charge-trapping sites be present [68, 69]. If these traps could be filled under forward bias working conditions, then it results in a good p- and n-contacts decreasing the charge recombination, which would improve the J_{sc} and FF [70, 71].

Moreover, the higher V_{oc} observed with the addition of P3HT or P3OT in the TiO_2-sensitized cells could be attributed to three processes: (1) an increase in the light absorption, (2) a shift in the TiO_2 CB, and/or (3) a change in the recombination rate. An increase in the photoabsorption will result in an increase in J_{sc} and produce, consequently, an increase of V_{oc}. However, in this case, the J_{sc} values are similar in both TiO_2/CdS/ZnS/P3HT and TiO_2/CdS/ZnS arrays, and hence, the increment of V_{oc} does not occur for this process. For the second effect, a shift in the TiO_2 CB produces a movement of the TiO_2 electron at quasi-Fermi level which determines the V_{oc}; then, an upward shift of the TiO_2 CB will mean an increase in the V_{oc}. Nevertheless, the same trend in the chemical capacitance is observed for the different configurations, Fig. 9a. For the third effect, the recombination rate can be also determined with EIS by analyzing the R_{rec}. An increase of this parameter indicates a reduction in the electron recombination process from the TiO_2 CB to the acceptor states, either in the electrolyte or the sensitizer [72]. This effect is observed in Fig. 9b where the R_{rec} increases with the addition of P3HT or P3OT, thus decreasing the recombination of charge carrier in the system and increasing the V_{oc}.

Another important parameter is the FF. Variations in this parameter can be due to the change in the transport resistance (R_t) [59, 72, 73]. It has been previously reported that R_t can vary depending on the sensitization process [59]. Analysis of the R_t behavior in the V_F convention (Fig. 9c), shows that R_t decreases with the addition of the polymers indicating an increment in the electron transport, which results in the increase of FF observed in Table 1.

No significant difference was noted between the use of P3HT and P3OT in the QDSSC with regard to the R_{rec} or R_t. Some studies have demonstrated that the charge mobility is higher in P3HT than that in P3OT [43, 55, 74]. That, in addition to the more uniform layer obtained, could be the reason for the higher J_{sc} on TiO_2/CdS/ZnS/P3HT, but at the same time, it may create a larger protecting layer between the TiO_2/CdS/ZnS array and the electrolyte, causing a lower FF compared with TiO_2/CdS/ZnS/P3OT array.

Other issue related to the use of conducting polymers in solar cells is the material stability [75]. It has been proven that the poly3-alkylthiophenes under UV–Vis light irradiation and thermal aging conditions result in the formation of oxidized species [76]. Moreover, it was established that oxygen forms a charge transfer complex with poly3-alkylthiophenes, which could be beneficial for the conductivity. Although most of the solar cells based on conducting polymers are tested under inert conditions, it is important to consider the performance and its relations under ambient conditions and stability. In this work, the hybrid QDSSCs were prepared and analyzed under ambient conditions; however, the rigorous stability tests are beyond the scope of this work. Further efforts are being carried out to improve the solar cell performance and to analyze the stability of the hybrid QDSSCs.

5 Conclusions

QDSSCs based on CdS/ZnS QDs and P3HT P3OT were analyzed. Either of the polymers added to the reference cell TiO_2/CdS/ZnS substantially increased V_{oc}, FF, and η. The V_{oc} values increased to 26 and 31 %, while the FF increased to 6 and 20 %, respectively, improving the conversion efficiency as a consequence. The polymer-coated photoanode enabled better protection between the QDs and the electrolyte, improving charge carrier transfer. Increased V_{oc} and FF values are the result of the reduction in the recombination processes (increment in R_{rec}) and the increment in the charge carrier's transport (decrement in R_t) obtained with the use of the polymers, as demonstrated by electrochemical impedance spectroscopy measurements. The difference between P3HT and P3OT offsets the improved J_{sc} for TiO_2/CdS/ZnS/P3HT and V_{oc} for TiO_2/CdS/ZnS/P3OT arrays; thus, the efficiency obtained was the same with either polymer. We can assume that poly-3-alkyl thiophenes and ZnS act similarly; however, the former enhances the solar cell performance.

Acknowledgments The authors acknowledge the financial support from the CONACYT through grant of the European Community Seven Framework Program (FP7-NMP-2010-EU-MEXICO) 263878; UC-MEXUS (00007); CIO-UGTO 2013–2015 (005/2013, 004/2014, 008/2015); CeMIE-Sol 27 and 28; and the CONACYT for the PhD scholarship for A. Cerdán-Pasarán and D. Esparza, and the postdoctoral fellow of I. Zarazúa and A. Martínez-Benítez. The authors also acknowledge Christian Albor for her technical support to obtain the SEM images.

References

1. Parida B, Iniyan S, Goic R (2011) A review of solar photovoltaic technologies. Renew Sustain Energy Rev 15:1625–1636. doi:10.1016/j.rser.2010.11.032
2. Panwar NL, Kaushik SC, Kothari S (2011) Role of renewable energy sources in environmental protection: a review. Renew Sustain Energy Rev 15:1513–1524. doi:10.1016/j.rser.2010.11.037
3. Saunders BR, Turner ML (2008) Nanoparticle-polymer photovoltaic cells. Adv Colloid Interface Sci 138:1–23. doi:10.1016/j.cis.2007.09.001
4. Zhu H, Wei J, Wang K, Wu D (2009) Applications of carbon materials in photovoltaic solar cells. Sol Energy Mater Sol Cells 93:1461–1470. doi:10.1016/j.solmat.2009.04.006
5. Xiao T, Fungura F, Cai M et al (2013) Improved efficiency and stability of inverted polymer solar cells with a solution-processed BPhen interlayer and polystyrene beads. Org Electron physics, Mater Appl 14:2555–2563. doi:10.1016/j.orgel.2013.06.019
6. Manoharan D, Chandrasekaran J, Maruthamuthu S, Jayamurugan P (2015) Poly(aniline-co-o-toluidine):poly(styrene sulfonic acid) nanocolloidal self assembled multilayer thin films as a hole transport layer in organic solar cells. Mater Sci Semicond Process 34:382–389. doi:10.1016/j.mssp.2015.02.079
7. Robel I, Subramanian V, Kuno M, Kamat PV (2006) Quantum dot solar cells. harvesting light energy with CdSe nanocrystals molecularly linked to mesoscopic TiO2 films. J Am Chem Soc 128:2385–2393. doi:10.1021/ja056494n
8. Rühle S, Shalom M, Zaban A (2010) Quantum-dot-sensitized solar cells. ChemPhysChem 11:2290–2304. doi:10.1002/cphc.201000069
9. Kamat PV (2007) Meeting the clean energy demand: nanostructure architectures for solar energy conversion. J Phys Chem C 111:2834–2860. doi:10.1021/jp066952u
10. Kouhnavard M, Ikeda S, Ludin NA et al (2014) A review of semiconductor materials as sensitizers for quantum dot-sensitized solar cells. Renew Sustain Energy Rev 37:397–407. doi:10.1016/j.rser.2014.05.023
11. Goh C, Scully SR, McGehee MD (2007) Effects of molecular interface modification in hybrid organic-inorganic photovoltaic cells. J Appl Phys. doi 10(1063/1):2737977
12. Antoniadou M, Stathatos E, Boukos N et al (2009) Study of hybrid solar cells made of multilayer nanocrystalline titania and poly(3-octylthiophene) or poly-(3-(2-methylhex-2-yl)-oxy-carbonyldithiophene). Nanotechnology 20:495201. doi:10.1088/0957-4484/20/49/495201
13. Luo J, Liu C, Yang S, Cao Y (2010) Hybrid solar cells based on blends of poly(3-hexylthiophene) and surface dye-modified, ultrathin linear- and branched-TiO2 nanorods. Sol Energy Mater Sol Cells 94:501–508. doi:10.1016/j.solmat.2009.11.013
14. Cappel UB, Dowland SA, Reynolds LX et al (2013) Charge generation dynamics in CdS:P3HT blends for hybrid solar cells. J Phys Chem Lett 4:4253–4257. doi:10.1021/jz402382e
15. Günes S, Sariciftci NS (2008) Hybrid solar cells. Inorganica Chim Acta 361:581–588. doi:10.1016/j.ica.2007.06.042
16. Martinez L, Stavrinadis A, Higuchi S et al (2013) Hybrid solution-processed bulk heterojunction solar cells based on bismuth sulfide nanocrystals. Phys Chem Chem Phys 15:5482–5487. doi:10.1039/c3cp50599e
17. Wright M, Uddin A (2012) Organic-inorganic hybrid solar cells: a comparative review. Sol Energy Mater Sol Cells 107:87–111. doi:10.1016/j.solmat.2012.07.006
18. Kim JP, Christians JA, Choi H et al (2014) CdSeS nanowires: compositionally controlled band gap and exciton dynamics. J Phys Chem Lett 5:1103–1109. doi:10.1021/jz500280g
19. Esparza D, Zarazúa I, López-Luke T et al (2015) Effect of Different Sensitization Technique on the Photoconversion Efficiency of CdS Quantum Dot and CdSe Quantum Rod Sensitized TiO 2 Solar Cells. J Phys Chem C 119:13394–13403. doi:10.1021/acs.jpcc.5b01525
20. Lopez-Luke T, Wolcott A, Xu LP et al (2008) Nitrogen-Doped and CdSe Quantum-Dot-Sensitized Nanocrystalline TiO2 Films for Solar Energy Conversion Applications. J Phys Chem C 112:1282–1292. doi:10.1021/jp077345p
21. Parsi Benehkohal N, González-Pedro V, Boix PP et al (2012) Colloidal PbS and PbSeS quantum dot sensitized solar cells prepared by electrophoretic deposition. J Phys Chem C 116:16391–16397. doi:10.1021/jp3056009
22. Yu WW, Qu L, Guo W, Peng X (2003) Experimental determination of the extinction coefficient of CdTe, CdSe, and CdS nanocrystals. Chem Mater 15:2854–2860. doi:10.1021/cm034081k
23. Shabaev A, Efros AL, Nozik AJ (2006) Multiexciton generation by a single photon in nanocrystals. Nano Lett 6:2856–2863. doi:10.1021/nl062059v
24. Beard MC, Knutsen KP, Yu P et al (2007) Multiple exciton generation in colloidal silicon nanocrystals. Nano Lett 7:2506–2512. doi:10.1021/nl071486l
25. Sambur JB, Novet T, Parkinson BA (2010) Multiple exciton collection in a sensitized photovoltaic system. Science 330:63–66. doi:10.1126/science.1191462
26. Hanna MC, Nozik AJ (2006) Solar conversion efficiency of photovoltaic and photoelectrolysis cells with carrier multiplication absorbers. J Appl Phys. doi 10(1063/1):2356795
27. Kamat PV (2013) Quantum dot solar cells. The Next Big Thing in Photovoltaics. J Phys Chem Lett 4:908–918. doi:10.1021/jz400052e
28. Zhao K, Pan Z, Mora-Seró I et al (2015) Boosting Power Conversion Efficiencies of Quantum-Dot-Sensitized Solar Cells Beyond 8% by Recombination Control. J Am Chem Soc 150416094653008:5602–5609. doi:10.1021/jacs.5b01946
29. Kongkanand A, Tvrdy K, Takechi K et al (2008) Quantum dot solar cells. Tuning photoresponse through size and shape control of CdSe–TiO2 architecture. J Am Chem Soc 130:4007–4015. doi:10.1021/ja0782706
30. Mor GK, Shankar K, Paulose M et al (2006) Use of highly-ordered TiO 2 nanotube arrays in dye-sensitized solar cells. Nano Lett 6:215–218. doi:10.1021/nl052099j
31. Badawi A, Al-Hosiny N, Abdallah S et al (2013) Tuning photocurrent response through size control of CdTe quantum dots sensitized solar cells. Sol Energy 88:137–143. doi:10.1016/j.solener.2012.11.005
32. Zarazúa I, De La Rosa E, López-Luke T et al (2011) Photovoltaic conversion enhancement of CdSe quantum dot-sensitized TiO2 decorated with Au nanoparticles and P3OT. J Phys Chem C 115:23209–23220. doi:10.1021/jp207744n
33. Chou C-Y, Lee C-P, Vittal R, Ho K-C (2011) Efficient quantum dot-sensitized solar cell with polystyrene-modified TiO2 photoanode and with guanidine thiocyanate in its polysulfide electrolyte. J Power Sources 196:6595–6602. doi:10.1016/j.jpowsour.2011.03.084
34. Yeh M-H, Lin L-Y, Lee C-P et al (2013) High performance CdS quantum-dot-sensitized solar cells with Ti-based ceramic materials as catalysts on the counter electrode. J Power Sources 237:141–148. doi:10.1016/j.jpowsour.2013.02.092
35. Jun HK, Careem MA, Arof AK (2013) Quantum dot-sensitized solar cells-perspective and recent developments: a review of Cd chalcogenide quantum dots as sensitizers. Renew Sustain Energy Rev 22:148–167. doi:10.1016/j.rser.2013.01.030
36. Esparza D, Oliva J, López-Luke T et al (2015) Current improvement in hybrid quantum dot sensitized solar cells by

increased light-scattering with a polymer layer. RSC Adv 5:36140–36148. doi:10.1039/C5RA03280F
37. Qiao Q, Beck J, Lumpkin R et al (2006) A comparison of fluorine tin oxide and indium tin oxide as the transparent electrode for P3OT/TiO2 solar cells. Sol Energy Mater Sol Cells 90:1034–1040. doi:10.1016/j.solmat.2005.05.020
38. Hao Y, Pei J, Wei Y et al (2010) Efficient semiconductor-sensitized solar cells based on poly(3-hexylthiophene)@CdSe@ZnO core-shell nanorod arrays. J Phys Chem C 114:8622–8625. doi:10.1021/jp911263d
39. Kim S, Im SH, Kang M et al (2012) Air-stable and efficient inorganic-organic heterojunction solar cells using PbS colloidal quantum dots co-capped by 1-dodecanethiol and oleic acid. Phys Chem Chem Phys 14:14999–15002. doi:10.1039/c2cp43223d
40. Gollu SR, Sharma R, Srinivas G et al (2015) Incorporation of SiO2 dielectric nanoparticles for performance enhancement in P3HT:PCBM inverted organic solar cells. Org Electron 24:43–50. doi:10.1016/j.orgel.2015.05.017
41. Freitas JN, Gonçalves AS, Nogueira AF (2014) A comprehensive review of the application of chalcogenide nanoparticles in polymer solar cells. Nanoscale 6:6371. doi:10.1039/c4nr00868e
42. Ren S, Chang L-Y, Lim S-K et al (2011) Inorganic-organic hybrid solar cell: bridging quantum dots to conjugated polymer nanowires. Nano Lett 11:3998–4002. doi:10.1021/nl202435t
43. Xiao X, Wang Z, Hu Z, He T (2010) Single crystals of polythiophene with different molecular conformations obtained by tetrahydrofuran vapor annealing and controlling solvent evaporation. J Phys Chem B 114:7452–7460. doi:10.1021/jp911525d
44. Huang H-L, Lee C-T, Lee H-Y (2015) Performance improvement mechanisms of P3HT:PCBM inverted polymer solar cells using extra PCBM and extra P3HT interfacial layers. Org Electron 21:126–131. doi:10.1016/j.orgel.2015.03.012
45. Mora-Seró I, Giménez S, Fabregat-Santiago F et al (2009) Recombination in quantum dot sensitized solar cells. Acc Chem Res 42:1848–1857. doi:10.1021/ar900134d
46. Guijarro N, Campiña JM, Shen Q et al (2011) Uncovering the role of the ZnS treatment in the performance of quantum dot sensitized solar cells. Phys Chem Chem Phys 13:12024–12032. doi:10.1039/c1cp20290a
47. Shen Q, Kobayashi J, Diguna LJ, Toyoda T (2008) Effect of ZnS coating on the photovoltaic properties of CdSe quantum dot-sensitized solar cells. J Appl Phys. doi 10(1063/1):2903059
48. Chen S, Paulose M, Ruan C et al (2006) Electrochemically synthesized CdS nanoparticle-modified TiO2 nanotube-array photoelectrodes: preparation, characterization, and application to photoelectrochemical cells. J Photochem Photobiol A Chem 177:177–184. doi:10.1016/j.jphotochem.2005.05.023
49. Wu Z, Zhao G, Zhang YN et al (2012) Enhanced photocurrent responses and antiphotocorrosion performance of Cds hybrid derived from triple heterojunction. J Phys Chem C 116:12829–12835. doi:10.1021/jp300374s
50. Jung SW, Kim JH, Kim H et al (2012) ZnS overlayer on in situ chemical bath deposited CdS quantum dot-assembled TiO 2 films for quantum dot-sensitized solar cells. Curr Appl Phys 12:1459–1464. doi:10.1016/j.cap.2012.04.012
51. Cerdán A, López-Luke T, Esparza D et al (2015) Photovoltaic Properties of Multilayered Quantum Dot/Quantum Rod-Sensitized TiO2 Solar Cells fabricated by SILAR and Electrophoresis. Phys Chem Chem Phys. doi:10.1039/C5CP02541A
52. Fabregat-Santiago F, Randriamahazaka H, Zaban A et al (2006) Chemical capacitance of nanoporous-nanocrystalline TiO2 in a room temperature ionic liquid. Phys Chem Chem Phys 8:1827–1833. doi:10.1039/b600452k
53. Beranek R (2011) (Photo)electrochemical Methods for the Determination of the Band Edge Positions of TiO2-Based Nanomaterials. Adv Phys Chem 2011:1–20. doi:10.1155/2011/786759
54. Mora-seró I, Fabregat-santiago F, Denier B et al (2006) Determination of carrier density of ZnO nanowires by electrochemical techniques. Appl Phys Lett 89:126–129. doi:10.1063/1.2390667
55. Savagatrup S, Printz AD, Wu H et al (2015) Viability of stretchable poly(3-heptylthiophene) (P3HpT) for organic solar cells and field-effect transistors. Synth Met 203:208–214. doi:10.1016/j.synthmet.2015.02.031
56. Galand EM, Kim Y, Mwaura JK et al (2006) Optimization of Narrow Band-Gap Propylenedioxythiophene: cyanovinylene Copolymers for Optoelectronic Applications Optimization of Narrow Band-Gap Propylenedioxythiophene : Cyanovinylene Copolymers for Optoelectronic Applications. Society 39:9132–9142. doi:10.1021/ma061935o
57. Li M, Ni W, Feng H et al (2015) A low bandgap carbazole based small molecule for organic solar cells. Org Electron 24:89–95. doi:10.1016/j.orgel.2015.05.024
58. González-Pedro V, Xu X, Mora-Seró I, Bisquert J (2010) Modeling high-efficiency quantum dot sensitized solar cells. ACS Nano 4:5783–5790. doi:10.1021/nn101534y
59. Fabregat-Santiago F, Garcia-Belmonte G, Mora-Seró I, Bisquert J (2011) Characterization of nanostructured hybrid and organic solar cells by impedance spectroscopy. Phys Chem Chem Phys 13:9083–9118. doi:10.1039/c0cp02249g
60. He C, Zheng Z, Tang H et al (2009) Electrochemical impedance spectroscopy characterization of electron transport and recombination in ZnO nanorod dye-sensitized solar cells. J Phys Chem C 113:10322–10325. doi:10.1021/jp902523c
61. Lee JK, Jeong BH, Jang SI et al (2009) Preparations of TiO2 pastes and its application to light-scattering layer for dye-sensitized solar cells. J Ind Eng Chem 15:724–729. doi:10.1016/j.jiec.2009.09.053
62. Samadpour M, Zad AI, Molaei M (2014) Simply synthesized TiO2 nanorods as an effective scattering layer for quantum dot sensitized solar cells. Chinese Phys B 23:047302. doi:10.1088/1674-1056/23/4/047302
63. Tian J, Lv L, Wang X et al (2014) Microsphere light-scattering layer assembled by ZnO nanosheets for the construction of high efficiency (>5%) quantum dots sensitized solar cells. J Phys Chem C 118:16611–16617. doi:10.1021/jp412525k
64. Itskos G, Papagiorgis P, Tsokkou D et al (2013) Size-dependent charge transfer in blends of Pbs quantum dots with a low-gap silicon-bridged copolymer. Adv Energy Mater 3:1490–1499. doi:10.1002/aenm.201300317
65. Unger EL, Hoke ET, Bailie CD et al (2014) Hysteresis and transient behavior in current–voltage measurements of hybrid-perovskite absorber solar cells. Energy Environ Sci 7:3690–3698. doi:10.1039/C4EE02465F
66. Meloni S, Moehl T, Tress W et al (2016) Ionic polarization-induced current–voltage hysteresis in CH3NH3PbX3 perovskite solar cells. Nat Commun 7:10334. doi:10.1038/ncomms10334
67. Kim HS, Jang IH, Ahn N et al (2015) Control of I-V Hysteresis in CH3NH3PbI3 Perovskite Solar Cell. J Phys Chem Lett 6:4633–4639. doi:10.1021/acs.jpclett.5b02273
68. Jeong YJ, Jang J, Song JH et al (2015) Charge transport characterization of PbS quantum dot solids for high efficiency solar cells. J Opt Soc Korea 19:272–276. doi:10.3807/JOSK.2015.19.3.272
69. Ruland A, Schulz-Drost C, Sgobba V, Guldi DM (2011) Enhancing photocurrent efficiencies by resonance energy transfer in CdTe quantum dot multilayers: towards rainbow solar cells. Adv Mater 23:4573–4577. doi:10.1002/adma.201101423
70. Snaith HJ, Abate A, Ball JM et al (2014) Anomalous Hysteresis in Perovskite Solar Cells. J Phys Chem Lett 5:1511–1515. doi:10.1021/jz500113x

71. Shao Y, Xiao Z, Bi C et al (2014) Origin and elimination of photocurrent hysteresis by fullerene passivation in CH3NH3PbI3 planar heterojunction solar cells. Nat Commun 5:1–7. doi:10.1111/j.1365-2230.2009.03702.x
72. Hod I, González-Pedro V, Tachan Z et al (2011) Dye versus quantum dots in sensitized solar cells: participation of quantum dot absorber in the recombination process. J Phys Chem Lett 2:3032–3035. doi:10.1021/jz201417f
73. De La Fuente MS, Sánchez RS, González-Pedro V et al (2013) Effect of organic and inorganic passivation in quantum-dot-sensitized solar cells. J Phys Chem Lett 4:1519–1525. doi:10.1021/jz400626r
74. Parlak EA (2012) The blend ratio effect on the photovoltaic performance and stability of poly (3-hexylthiophene):[6,6]-phenyl-C61 butyric acid methyl ester (PCBM) and poly(3-octylthiophene):PCBM solar cells. Sol Energy Mater Sol Cells 100:174–184. doi:10.1016/j.solmat.2012.01.011
75. Arenas MC, Mendoza N, Cortina H et al (2010) Influence of poly3-octylthiophene (P3OT) film thickness and preparation method on photovoltaic performance of hybrid ITO/CdS/P3OT/Au solar cells. Sol Energy Mater Sol Cells 94:29–33. doi:10.1016/j.solmat.2009.04.013
76. Manceau M, Rivaton A, Gardette JL et al (2009) The mechanism of photo- and thermooxidation of poly(3-hexylthiophene) (P3HT) reconsidered. Polym Degrad Stab 94:898–907. doi:10.1016/j.polymdegradstab.2009.03.005